

crevice corrosion is related to the known localized, corrosion-resistance properties of the Ni-Cr-Mo-based composition of the Ni-Cr-Mo-Gd alloy.

### 3.1.1 Additional PD Testing Results

Figure 7 shows cyclic PD polarization scans for the four borated stainless steel specimens in B1 solution (see Tables 1 and 3). The solution was purged with  $N_2$  during the entire test period. A 50-min  $E_{corr}$  measurement was performed before initiating the test sequence. The dotted line in Figure 7 indicates the breakdown threshold using a  $10 \mu A/cm^2$  criterion. Table 5 contains parameters obtained from the corrosion potential ( $E_{corr}$ ) and PD curves. Note that the 304B5 has the most positive breakdown potential ( $E_{bd}$ ), and the repassivation potential ( $E_{rp}$ ) value is very similar to 304B4 (best performing). This observation is consistent with the low number of negative spikes in the aerated  $E_{corr}$  measurements for 304B5. The A978 specimen has the most negative values for  $E_{bd}$  and  $E_{rp}$  (worst performing). The 304B6 has a similar  $E_{bd}$  to 304B4 but has a much more negative  $E_{rp}$  that is similar to the A978. Because the 304B6 has significantly more B content than A978, the similar  $E_{rp}$  value indicates a microstructural effect. Thus, these tests show that the amount of boron and the alloy grade (microstructure) influence the localized-corrosion characteristics. In all cases, significant pitting was observed under the crevice formers. In some cases, pitting was observed on boldly exposed surfaces as well.

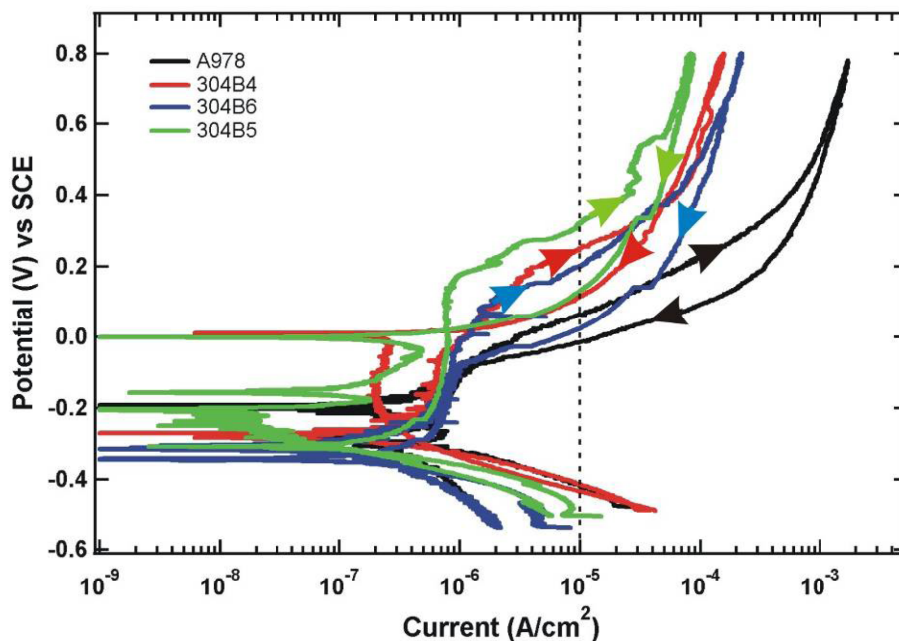


Figure 7. PD curves for borated SS alloys in solution B1 at 60°C.

Table 5. Parameters obtained from PD curves in solution B1.

	304B4	304B5	304B6	A978
$E_{corr}$	-0.28	-0.3034	-0.3347	-0.291
$E_{bd}$	0.25	0.321	0.207	0.055
$E_{rp}$	0.022	0.018	-0.0943	-0.115

Additional PD tests were performed for the three Neutrosorb Plus alloys in solution B3 using Teflon MCA crevice formers. The curves from these tests are shown in Figure 8, with the data tabulated in Table 6. The  $E_{\text{corr}}$  values follow the trend of decreasing with increasing boron level. The  $E_{\text{bd}}$  potentials do not follow the trend of boron content because 304B5 has a higher  $E_{\text{bd}}$  value than 304B4. The  $E_{\text{rp}}$  values decrease with increasing boron level, as expected. A comparison of the alloys in the two solution types shows only a slight depression of the  $E_{\text{corr}}$  and  $E_{\text{rp}}$  values in B3, which is a significantly lower  $\text{NO}_3/(\text{Cl}+\text{F})$  value. The  $E_{\text{bd}}$  values are actually higher in the B1 solution, which is counter to the effect of halides. It is thought that at these low ionic contents the concentration of halides, which contribute to enhanced corrosion, must be less of an influence in localized corrosion processes. More testing would be required to make any significant statements about these results because they are based on single observations.

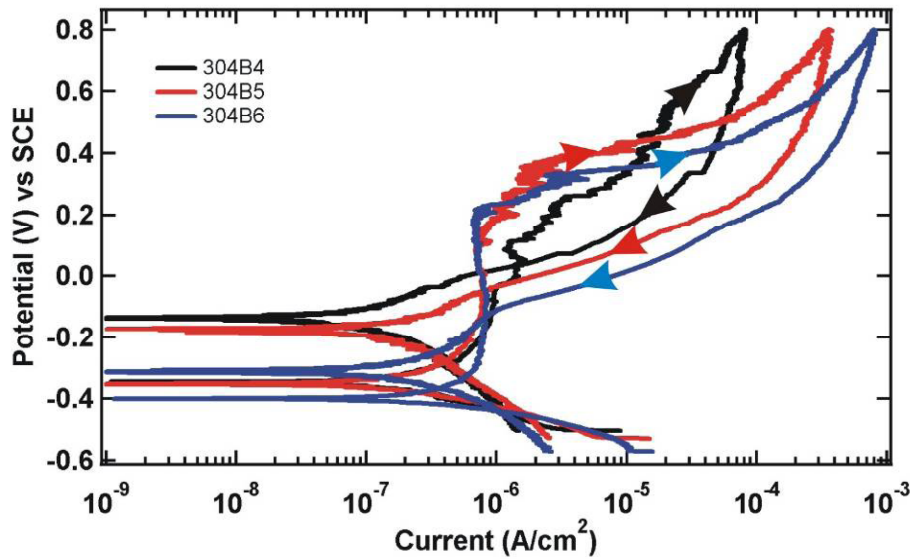


Figure 8. PD curves in solution B3 using Teflon multiple crevice assembly (MCA) crevice formers.

Table 6. Parameters obtained from PD curves in B3 solution.

	304B4	304B5	304B6
$E_{\text{corr}}$	-0.3031	-0.3283	-0.3728
$E_{\text{bd}}$	0.351	0.429	0.353
$E_{\text{rp}}$	0.032	-0.052	-0.137

## 3.2 PS Tests

### 3.2.1 PS Test Introduction

PS tests were used to determine the corrosion performance of the alloys over longer periods. In the case where no localized corrosion occurs, the current from the PS tests is directly proportional to the general corrosion rate. In the event that localized corrosion occurs during the PS test, the situation is not as straightforward. As localized corrosion by definition is not a uniform mechanism, the rate will not have the same meaning, but it is still proportional to the amount of material being removed. The rate is reported as a general corrosion rate in either case. The basis for calculation of the corrosion rate from the corrosion current ( $i_{\text{corr}}$ ) can be found in ASTM G102<sup>21</sup> and is derived from Faraday's Law. As stated previously, the

corrosion rate assumes a uniform loss of material, which does not occur with localized processes, such as pitting, crevice corrosion, or dissolution of a secondary phase (i.e., the gadolinide phase in the Ni-Cr-Mo-Gd alloy).

The electrochemical potential chosen for the PS tests is based on what is expected in the environment. This was determined by measuring the  $E_{\text{corr}}$  for 24 hours while it was being saturating with air. This mimics the effect of maximum exposure of air, where oxygen acts as an oxidizer to shift the potentials of the materials in a positive direction. While general corrosion does not have a strong potential dependence, localized-corrosion initiation/propagation tends to increase with potential. The actual potential used for the tests was based on an early test for a 304B4 specimen where the  $E_{\text{corr}}$  value appeared to equilibrate between 0 and 0.1 V. Thus, while most of the tests were performed at 0.1 V, 0.2 V was also tested because higher aerated  $E_{\text{corr}}$  values for 304B4 were observed in other tests.

The PS curves obtained from these measurements also provide qualitative information. Ideally, general corrosion is a smooth current flow that decreases exponentially during the test. This has been observed in long-term corrosion testing of passive materials proposed for use by the YMP.<sup>22</sup> Localized corrosion can be ascertained if there are increases in current during the test. Metastable pitting events (the origins of pitting or crevice corrosion) are characterized by short-lived positive spikes in the current trace. Longer-lived events, beyond several seconds, are the result of sustained localized corrosion. The total charge is the integration of the current over the entire PS test. This provides a value for the total amount of material removed assuming the current is due to corrosion processes.

In addition, three LPR measurements were made just prior to the PS tests. These tests were performed after  $N_2$  degassing for 24 hours to allow equilibration. The test involves scanning the potential at a slow scan rate (0.166 mV/sec), from -30 mV to +30 mV versus the measured  $E_{\text{corr}}$ . ASTM G59<sup>23</sup> describes the use of this technique in determining  $i_{\text{corr}}$  at open circuit potential ( $E_{\text{corr}}$ ) using the Butler-Volmer relationship.<sup>24</sup> The slope of the curve is the polarization resistance ( $R_p$ ) and has units of  $\Omega\text{-cm}^2$ . The value of  $i_{\text{corr}}$  can be calculated if the Stern-Geary coefficient (B) is known. The three values were evaluated using the software package provided with the instrumentation. The linear portion of each curve was fit to determine the polarization resistance (slope of I-V curve). This was multiplied by the exposed surface area of the specimen. The value of (B) was estimated using Tafel slopes of 0.12 V/dec, yielding  $B = 0.0261$  V. The  $i_{\text{corr}}$  was calculated using ASTM G59 Equation 2. The corrosion rate was calculated from  $i_{\text{corr}}$  as described previously for PS tests. A more advanced treatment uses a fitting procedure to determine the parameters in the event Tafel slopes are not known.<sup>25</sup> The corrosion rate is then calculated using the  $i_{\text{corr}}$  values, as described for the PS tests. Use of this method was not considered after very low cathodic Tafel slopes (below 5 mV/dec in most cases) were obtained. This is thought to be an issue with the software method of performing the sweep, where the step is immediately followed by the sweep. The fast drop in current and, consequentially, the low-calculated Tafel slope is due to capacitive discharge of the interface. Future studies will use a delay before the sweep is initiated.

The data for PS tests are contained in Table 7. Data from the A978 specimens are included in Appendix A. This should be referred to for the data sections that follow. In some cases, tests were interrupted by power failure (Tests 080806-1 and 080806-2) or problems with the reference electrode (Tests 080906-1 and 082106). The available data for these particular tests was placed in Table 7.

Table 7. Data obtained from electrochemical tests for borated stainless steel and Ni-Cr-Mo-Gd alloy.

Test ID	Alloy	Solution	Final $E_{\text{corr}}$ Ox (V)	Final $E_{\text{corr}}$ N <sub>2</sub> (V)	Potential (V)	Total Charge (C/cm <sup>2</sup> )	Peak Current (A/cm <sup>2</sup> )	$i_{\text{corr}}$ (A/cm <sup>2</sup> )	CR <sup>a</sup> ( $\mu\text{m}/\text{yr}$ )
072406	304B4	B1	0.0331	-0.3011	0.1	4.44E-03	4.76E-06	3.42E-09	0.0325
072506	304B4	B3	0.0281	-0.3972	0.1	5.68E-03	6.69E-06	2.84E-09	0.0270
072606	304B4	B1	0.1781	0.04428	0.1	2.40E-03	2.03E-07	2.54E-09	0.0242
080806-1	304B4	B1	0.0697	-0.2493	0.1	N/A	N/A	N/A	N/A
080806-2	304B4	B1	0.1308	-0.1203	0.2	N/A	N/A	N/A	N/A
080906-1	304B4	B3	0.008	-0.29	0.1	3.65E-2	1.12E-04	1.24E-8	0.118
081406	Ni-Cr- Mo-Gd	B1	- 0.3186	-0.3264	0.1	4.01	2.26E-04	1.63E-06	16.3
081706	Ni-Cr- Mo-Gd	B3	-0.259	-0.277	0.1	1.85	8.08E-5	1.01E-6	7.02
082106	Ni-Cr- Mo-Gd	B1	- 0.3165	-0.3193	0.2	1.62	3.87E-4	9.36E-6	93.8
082406	Ni-Cr- Mo-Gd	B3	- 0.2869	-0.3005	0.2	2.19	1.32E-4	3.49E-7	3.50

**Notes:** (numbers in red are incomplete data)

Tests 080806-1 and 080806-2 were interrupted by power outages, and potentiostatic (PS) data was lost

Test 080906-1 was interrupted by reference electrode problem after 2.07 days

Test 082106 was interrupted after 12 hours due to a bubble in the Luggin capillary

a. CR: corrosion rate

### 3.2.2 $E_{\text{corr}}$ Measurements

The  $E_{\text{corr}}$  values measured under aeration demonstrated vastly different results for the borated stainless steels and the Ni-Cr-Mo-Gd alloy. The  $E_{\text{corr}}$  values were observed to shift positive of -0.1 V for the 304B4 alloy and as far positive as 0.178 V (Test 072606). Most tests showed  $E_{\text{corr}}$  values for 304B4 under aerated conditions between 0 and 0.2 V. These values should not be considered equilibrated because the potentials were trending positive at the end of the test. The values decreased to between -0.4 V and -0.25 V after the N<sub>2</sub> gas purge. The  $E_{\text{corr}}$  for the Ni-Cr-Mo-Gd was unaffected by the aeration, with observed values near -0.3 V. Examples of  $E_{\text{corr}}$  versus time are shown for conditions of aeration (see Figure 9) and N<sub>2</sub> gas purge (see Figure 10). The  $E_{\text{corr}}$  for the 304B4 alloy shows numerous negative excursions while being aerated. These are due to metastable (short-lived) pitting events. The  $E_{\text{corr}}$  for the Ni-Cr-Mo-Gd alloy does not show this type of activity, likely due to the corrosion potential being pinned to more negative potentials, which is due to the dissolution of the gadolinide phase.

Using the measured  $E_{\text{corr}}$  values observed for the 304B4 alloy, the potential for the PS tests was chosen to be 0.1 V. One test for 304B4, Test 072606, had a final  $E_{\text{corr}}$  value above 0.1 V. As will be discussed in Section 3.2.5, PS Measurements, a more positive value of 0.2 V was investigated as well. While the Ni-Cr-Mo-Gd showed much more negative values for  $E_{\text{corr}}$ , it is anticipated that the eventual removal of the surface intersecting gadolinide phase would result in  $E_{\text{corr}}$  values more like that of the 304B4.

Four tests were performed for the A978 alloy but are not shown. These tests had issues with specimen contacts, which are discussed in Section 3.2.5.

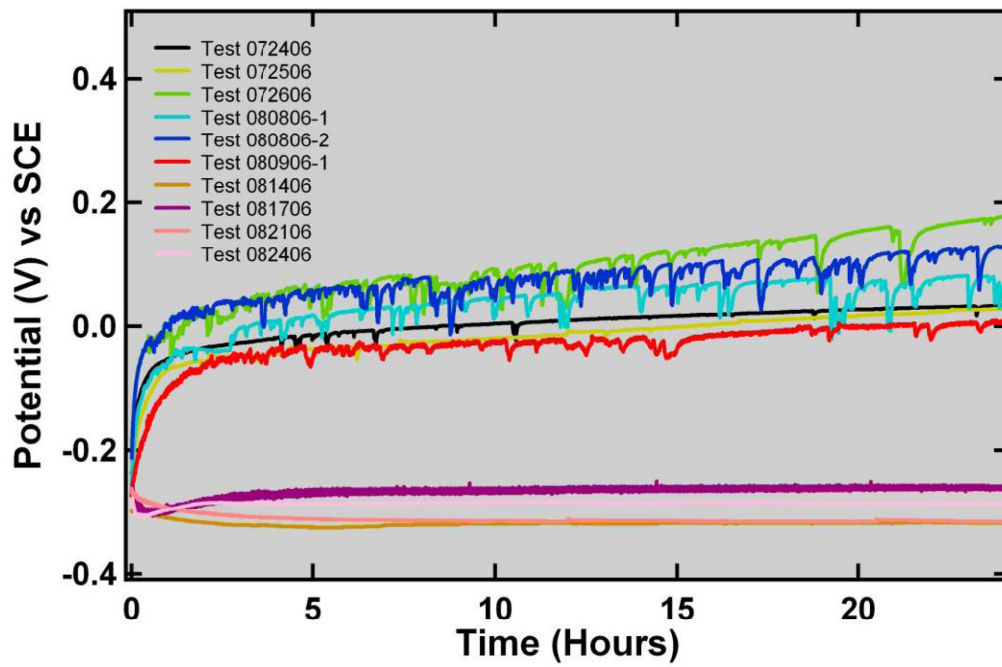


Figure 9.  $E_{\text{corr}}$  versus time for aerated cell. Tests 072406, 072506, 072606, 080806-1, 080806-2, and 080906-1 are 304B4 specimens and test 081406, 081706, 082106, and 082406 are Ni-Cr-Mo-Gd specimens.

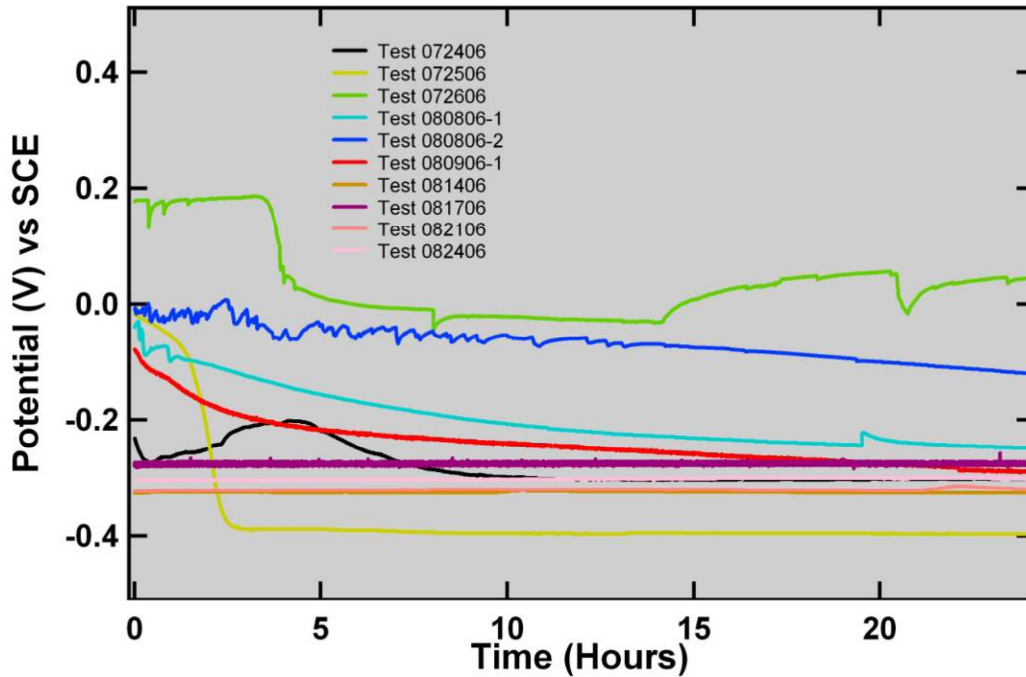


Figure 10.  $E_{\text{corr}}$  versus time for  $\text{N}_2$  purged cell. Test 072406, 072506, 072606, 080806-1, 080806-2, and 080906-1 are 304B4 specimens, and tests 081406, 081706, 082106, and 082406 are Ni-Cr-Mo-Gd specimens.

### 3.2.3 Additional Testing of Long-Term $E_{\text{corr}}$ Tests

To determine the long-term  $E_{\text{corr}}$  value under aeration for 304B4 and 304B5 specimens, the  $E_{\text{corr}}$  was measured continuously for four consecutive 1-week periods at  $60^\circ\text{C}$ . Short gaps exist (up to several hours) where data was not collected. However, the data is plotted without these time gaps. Also note that the main specimen glassware joint showed condensation and precipitate from evaporative loss through that joint. Nanopure water was added to replace the water loss on a weekly basis. The precipitate was analyzed by XRD and was primarily  $\text{NaCl}$  and  $\text{NaNO}_3$ . Thus, the ionic composition was diluted over the testing period.

Figure 11 shows a plot of the data for specimens 304B5 and 304B6. The potential of both specimens rose in the initial hours to over 0 V, with 304B6 attaining the more positive value. The 304B6 specimen also had a significant number of negative spikes due to localized corrosion. After 2 weeks, some of the negative spikes are up to 0.3 V in magnitude and last for many hours. The 304B5 specimen showed few negative excursions comparatively. After 1 week, two LPR scans were performed on the 304B6 specimen while under aeration. The corrosion rate was  $80 \pm 3$  nm/yr, indicating very low general corrosion rate in the passive region compared to those measured under  $\text{N}_2$  purge in the PS tests, where the  $E_{\text{corr}}$  values were much more negative. The lower corrosion rate is due to the specimen residing in the passive region when aerated. After the tests, the specimen was examined with LOM, as shown in Figure 12. The most significant damage was observed at the Teflon compression gasket, where pitting around the circumference of the gasket was observed. Other less extensive pitting damage was observed under the MCA crevice formers. No significant damage to the 304B5 specimen with a ceramic MCA was observed.

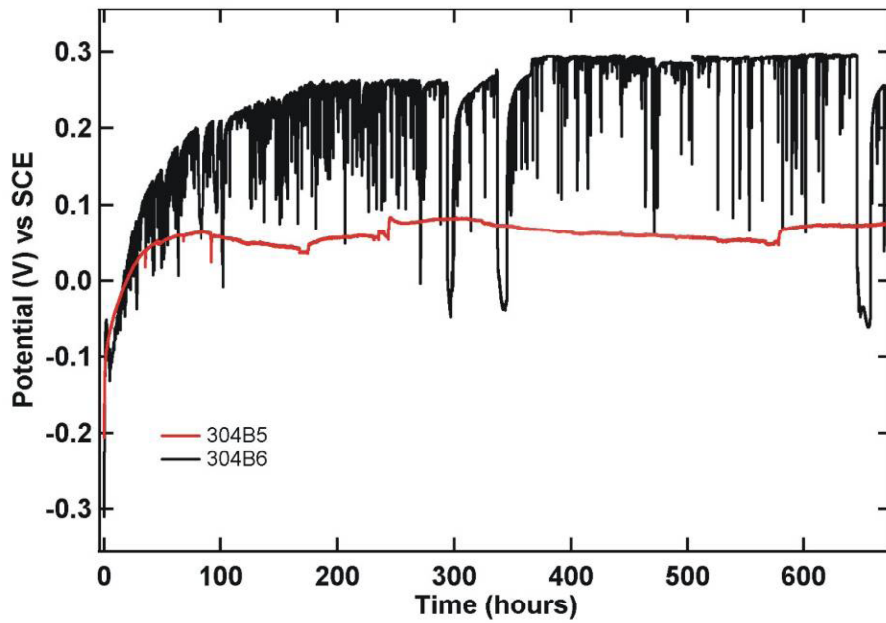


Figure 11.  $E_{\text{corr}}$  versus time for 304B5 and 304B6 specimens in solution B3 at 60°C.

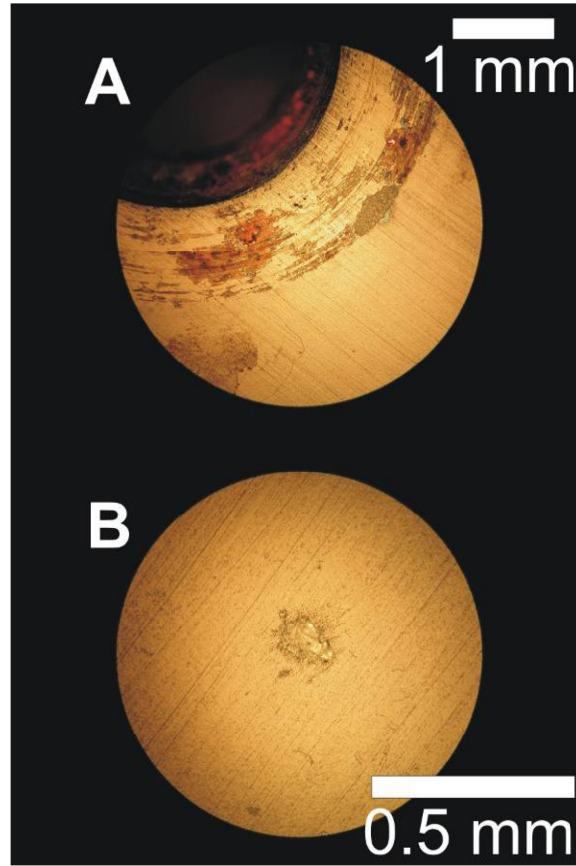


Figure 12. LOM of 304B6 specimen after 4 weeks at  $E_{\text{corr}}$ . Image (A) was taken from a compression gasket (50 $\times$ ) and image (B) was taken from an area under the MCA crevice former (200 $\times$ ).

An additional test using a 304B5 specimen was performed with a Teflon MCA and showed more negative excursions and a final potential that exceeded 0.2 V. This specimen did show limited crevice corrosion damage under the washer.

### 3.2.4 LPR Measurements

The corrosion rates calculated for LPR curves show that the 304B4 has lower corrosion rates than the Ni-Cr-Mo-Gd alloy. It is believed that the indicated corrosion rates for the Ni-Cr-Mo-Gd alloy are actually measuring the dissolution of the gadolinide secondary phase and are not indicative of the general corrosion rate of the base material. Table 8 shows the corrosion rates calculated from the LPR data. These results show the same trends observed in the PS tests described in Section 3.2.6.

Table 8. Corrosion rates from linear polarization resistance (LPR) measurements.

Test ID	Specimen Type	Avg. CR ( $\mu\text{m}/\text{yr}$ )	SD
72406	304B4	0.221	0.070
72506	304B4	0.276	0.057
72606	304B4	0.067	0.005
080806-1	304B4	0.197	0.072
080806-2	304B4	0.115	0.011
080906-1	304B4	0.647	0.049
81406	Ni-Cr-Mo-Gd	24.1	3.1
81706	Ni-Cr-Mo-Gd	5.19	0.067
82106	Ni-Cr-Mo-Gd	21.1	1.8
82406	Ni-Cr-Mo-Gd	1.85	0.960

### 3.2.5 PS Measurements

The PS measurements were performed primarily at 0.1 V, with 0.2 V used to determine the effect of higher potential in some tests. These values were derived from the  $E_{\text{corr}}$  measurements under aeration as described in Section 3.2.4. Figure 13 shows a plot of curves for the 304B4 and Ni-Cr-Mo-Gd alloys. In the case of 304B4, the current dropped to very low values at both potentials. The current translated into corrosion rates of less than 100 nm/year, which indicate very passive behavior. Spikes up to several hundred  $\text{nA}/\text{cm}^2$  were observed during the tests, indicating metastable pitting activity, but no long-lived current excursions were observed. The total charge values were also very low, which is another indication that very little corrosion had occurred. Test 080806-2 was run at a higher potential of 0.2 V with similar behavior; however, a power outage resulted in the test ending early, and the data was lost. The data for the Ni-Cr-Mo-Gd alloy indicated lower general corrosion performance. This is likely due to the slow dissolution of the gadolinide phase. Steady decreases in current were observed for all Ni-Cr-Mo-Gd alloy tests. Longer test times or secondary-phase removal prior to testing should be considered to evaluate the true performance of the Ni-Cr-Mo-Gd alloy.

The four tests that were run with the A978 alloy are not shown in Figure 13 due to issues with these tests stemming from the design of the electrical contact. The first two tests used the epoxy-coated contacts, which delaminated after several days of exposure. After delamination, the contact corroded and contributed to the measured current. The second two tests used an exposed platinum wire contact that appeared to affect the potential and current during the tests. Small negative currents were observed for these final tests that are likely indicative of reactions on platinum. One crevice corrosion site was observed for Test 080206.

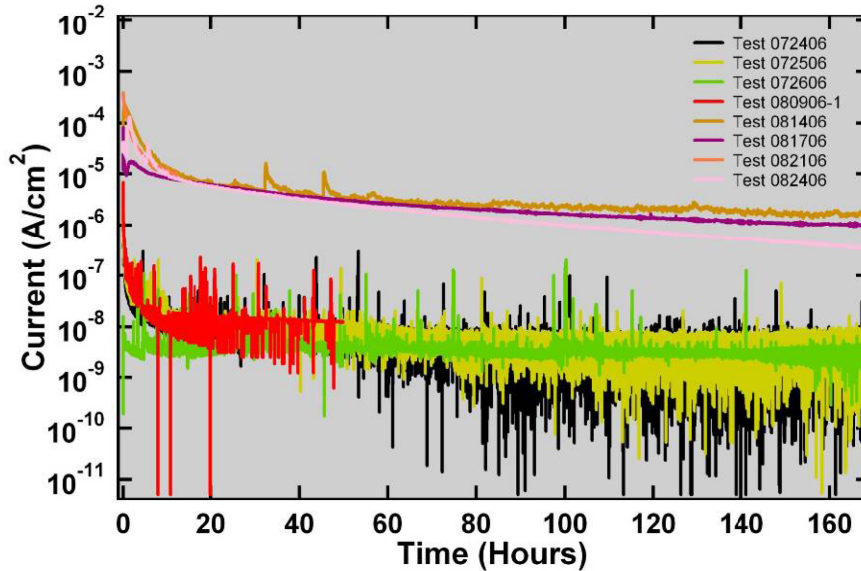


Figure 13. Current versus time plots for potentiostatic (PS) tests. Test 072406, 072506, 072606, and 080906-1 are for 304B4 specimens, and Tests 081406, 081706, 082106, and 082406 are Ni-Cr-Mo-Gd specimens. Note that Tests 080906-1 and 082106 are not complete 7-day data sets.

### 3.2.6 Additional PS Testing of Borated Stainless Steel at 60°C

Additional PS tests were performed on specimens of 304B4, 304B5, and 304B6 using the protocol employed in FY-06 testing of neutron absorbing alloys: (1) measurement of  $E_{\text{corr}}$  under aeration for 24 hours, (2) measurement of  $E_{\text{corr}}$  under  $\text{N}_2$  purge for 24 hours, (3) followed by three LPR scans, and (4) 7-day PS hold at 0.1 or 0.2 V versus SCE.<sup>26</sup> The testing was performed in solution B3.

Figure 14 shows the  $E_{\text{corr}}$  data for 304B4, 304B5, and 304B6 under aeration and  $\text{N}_2$  purge. The  $E_{\text{corr}}$  increases with time under aeration into the passive region. The negative excursions are localized corrosion initiations. The 304B6 specimen showed much more activity than the lower boron-containing alloys. Purging with  $\text{N}_2$  resulted in the potential dropping to below -0.3 V versus SCE.

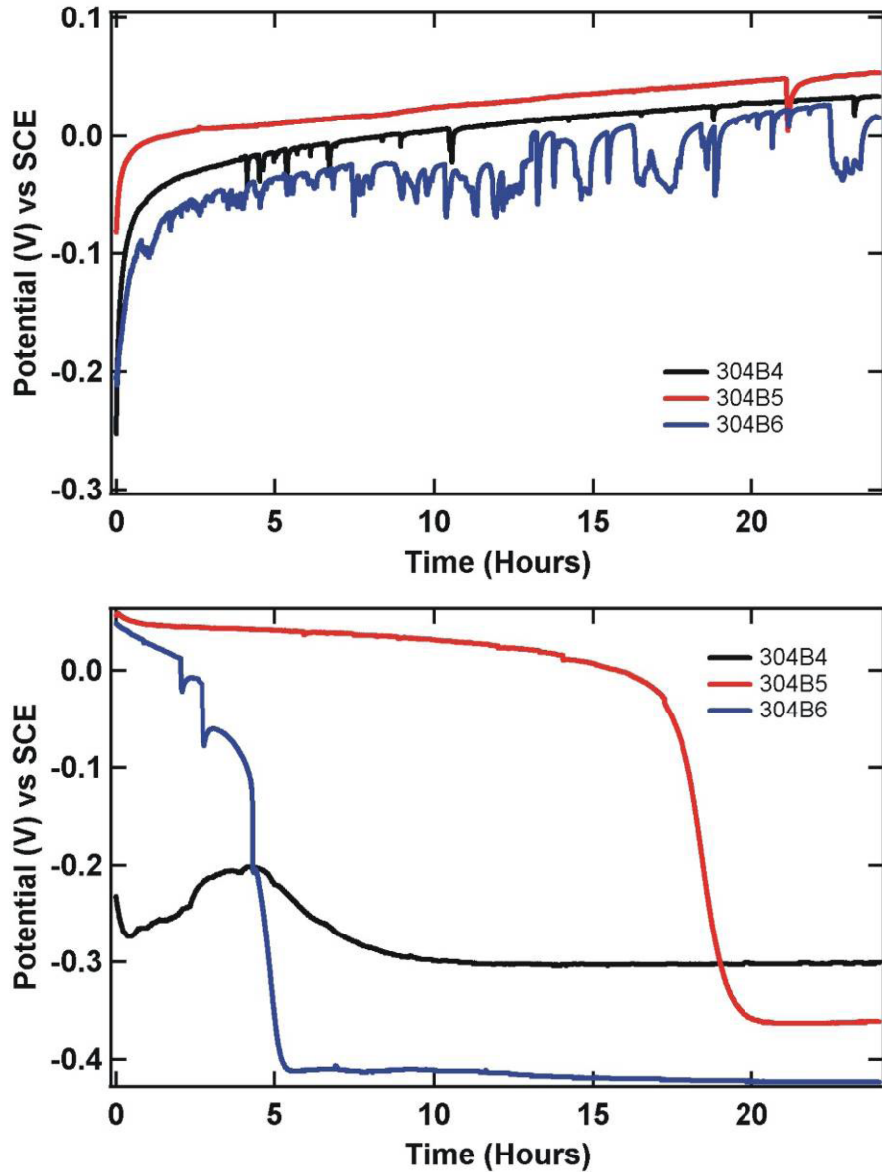


Figure 14.  $E_{\text{corr}}$  for 304B4, 304B5, and 304B6 in solution B3 at 60°C with air (top) and  $\text{N}_2$  (bottom) purge.

The LPR calculated corrosion rates under  $\text{N}_2$  purge were determined using three curves. The average corrosion rates obtained from fitting were  $221 \pm 70$  nm/yr for 304B4 (from FY-06 testing),<sup>26</sup>  $427 \pm 132$  nm/yr for 304B5, and  $464 \pm 100$  nm/yr for 304B6.

The PS curves for the three Neutrosorb Plus alloys are shown in Figure 15. The alloys with lower boron content (304B4, 304B5) show passivation during the test while the 304B6 shows much higher current, particularly at the end of the test where crevice corrosion was observed. This specimen was coated with a thick iron-oxide film. While small pits were observed under the MCA crevice formers, the most significant corrosion was observed at the Teflon compression fitting used to isolate the specimen electrical contact. One PS experiment was performed for 304B5 with Teflon MCA washers at 0.1 V versus SCE. Figure 16 shows significant current increase initiated during the test that was consistent with crevice corrosion under the MCA in post-test inspection.

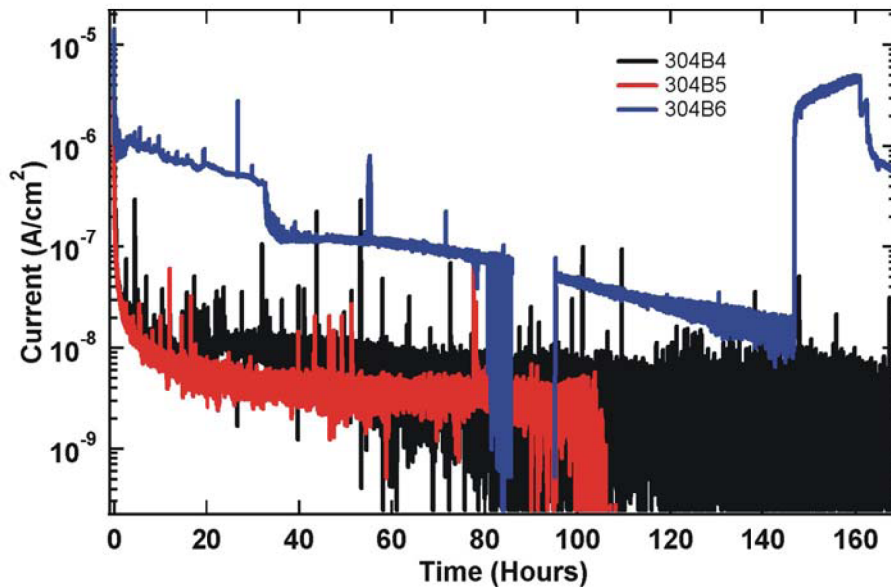


Figure 15. PS curves for 304B4, 304B5, and 304B6 in solution B3 with ceramic MCA.

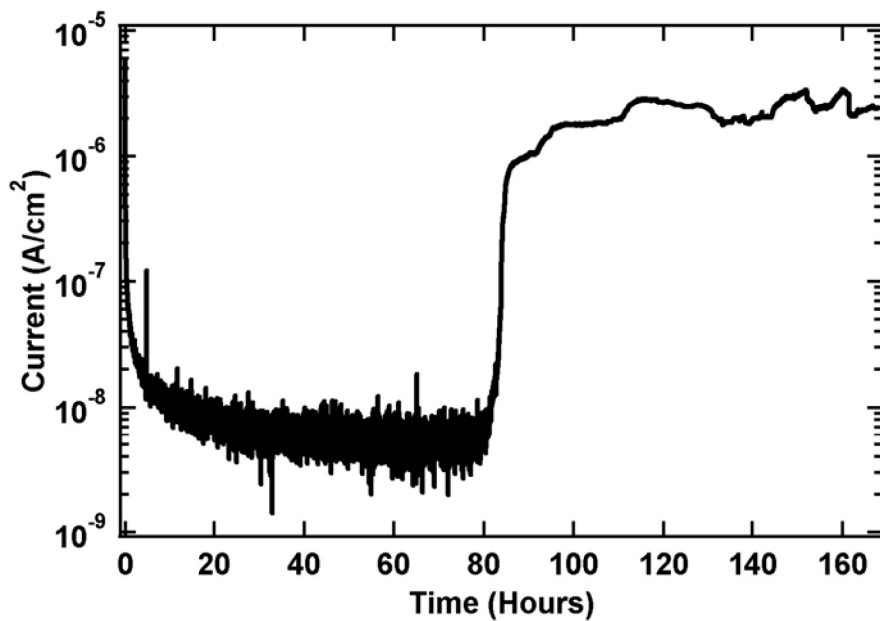


Figure 16. PS curve for 304B5 in solution B3 with Teflon MCA.

### 3.2.7 Additional PS Testing for Nickel-based Alloys at 90°C

Data from the electrochemical tests is shown in Table 9. The  $E_{\text{corr}}$  was greatest for the Alloy 22 specimen and somewhat lower for the Ni-Cr-Mo-Gd alloys. The total charge was much higher for the M340 alloy (lowest chromium level), with Alloy 22 having the lowest overall charge passed during the test. From the final value of the PS tests, the corrosion ( $I_{\text{corr}}$ ) rate was calculated. This approach can have some error due to the random fluctuation in the corrosion current due to crevice corrosion events. A value of the corrosion rate based on the weight loss during the test is also calculated. Figure 17 shows a plot of the current for these three alloys. The Alloy 22 specimen showed the highest passivity at the early stages of the test. However, at later times, crevice corrosion was initiated and an increase in the current to levels similar to the Ni-Cr-Mo-Gd were observed.

Table 9. Data from electrochemical tests (Ni-based alloy tests).

Alloy	$E_{\text{corr}}$ (V)	Total Charge (C/cm <sup>2</sup> )	$I_{\text{corr}}$ (A/cm <sup>2</sup> )	$I_{\text{corr}}$ CR (μm/yr)	Weight Loss (mg)	CR from gravimetric analysis (μm/yr)
M340	-0.4409	3.22	3.39E-06	34.3	12.62	47.2
M327	-0.4468	1.37	1.07E-06	10.4	5.46	19.6
Alloy 22	-0.3962	1.12	2.08E-06	20.2	4.11	15.7

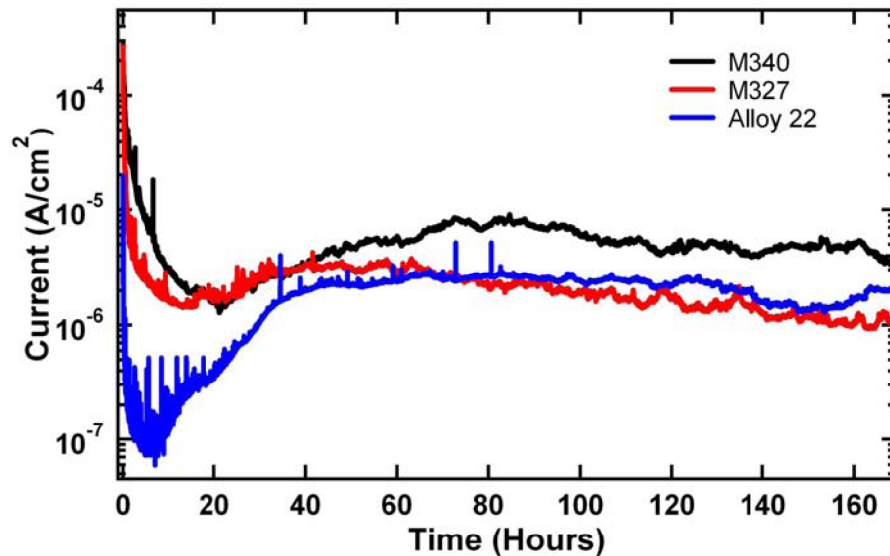


Figure 17. Current traces during PS tests.

### 3.2.8 Post-Test Analysis of PS Test Specimens

After the tests, analysis of the specimens and test solutions involved visual inspection, gravimetric analysis, LOM, and SEM. Table 10 provides brief post-test observations for the 304B4 and Ni-Cr-Mo-Gd specimens. The solutions were clear and colorless, except for Test 082106 where the reference electrode failed, resulting in unknown potentials (transpassive corrosion). This solution was yellow from dissolved

chromate ions. The specimens were free of extensive damage to the surface and were shiny, with evidence of slight hazing due to secondary-phase removal for the Ni-Cr-Mo-Gd specimens (see Figure 18). Some of the Ni-Cr-Mo-Gd specimens showed staining under the crevice former as a result of gadolinide removal.

Table 10. Post-test PS test observations.

Test ID	Alloy	Solution	Solution Observations	Specimen Observations
072406	304B4	B1	Clear and colorless	One small crevice pit
072506	304B4	B3	Clear and colorless	Light pitting under several crevice formers
072606	304B4	B1	Clear and colorless	one crevice area (etched)
080806-1	304B4	B1	Clear and colorless	Etching under several crevice formers
080806-2	304B4	B1	Clear and colorless	Etching and pitting under several crevice formers
080906-1	304B4	B3	Clear and colorless	No crevice corrosion
081406	Ni-Cr-Mo-Gd	B1	Clear and colorless	Partial surface gadolinide removal
081706	Ni-Cr-Mo-Gd	B3	Clear and colorless	Partial surface gadolinide removal
082106	Ni-Cr-Mo-Gd	B1	Clear and yellow	Heavy etching on boldly exposed surface, removal of surface gadolinides
082406	Ni-Cr-Mo-Gd	B3	Clear and colorless	Partial surface gadolinide removal

Representative LOM images of the damage from each of these alloys are shown in Figure 18. In several cases, small pits or light etching was observed under a crevice former for 304B4 specimens (see Figure 18). The most damage was observed for Tests 080806-1 and 080806-2, which were incomplete and are not shown. For the Ni-Cr-Mo-Gd tests, the removal of the gadolinide phase was partial for completed tests (Tests 081406, 081706, 082406). No evidence of primary phase corrosion was found for the Ni-Cr-Mo-Gd alloys. Figure 19 shows that there was a partial removal of the gadolinide secondary phase for Test 081406.

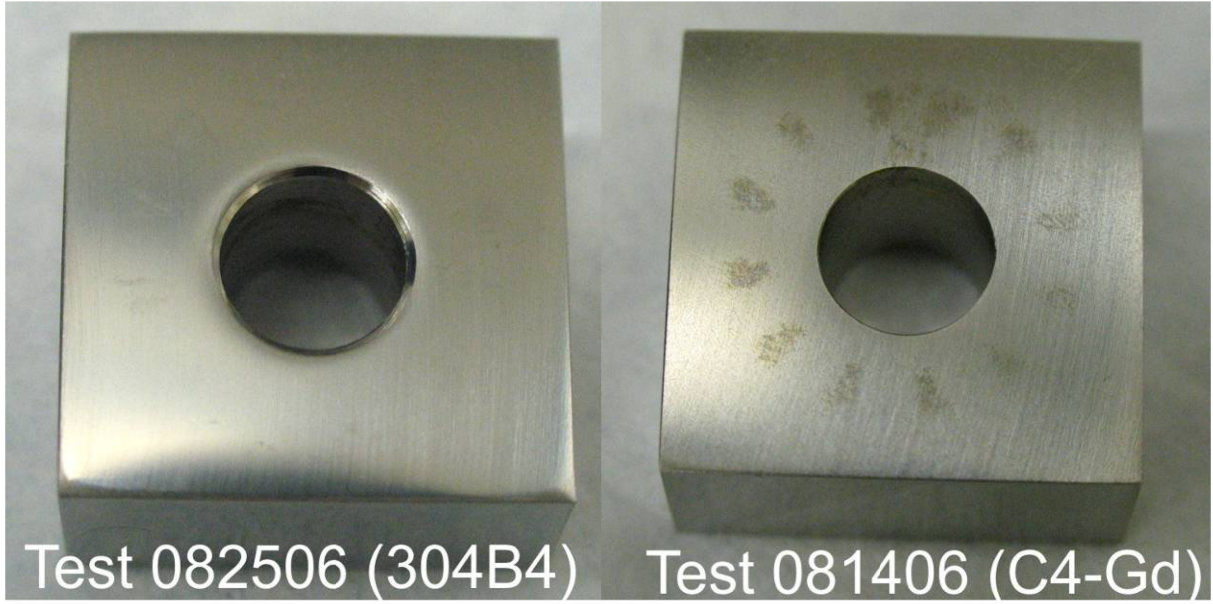


Figure 18. Photographs of PS test specimens after testing.

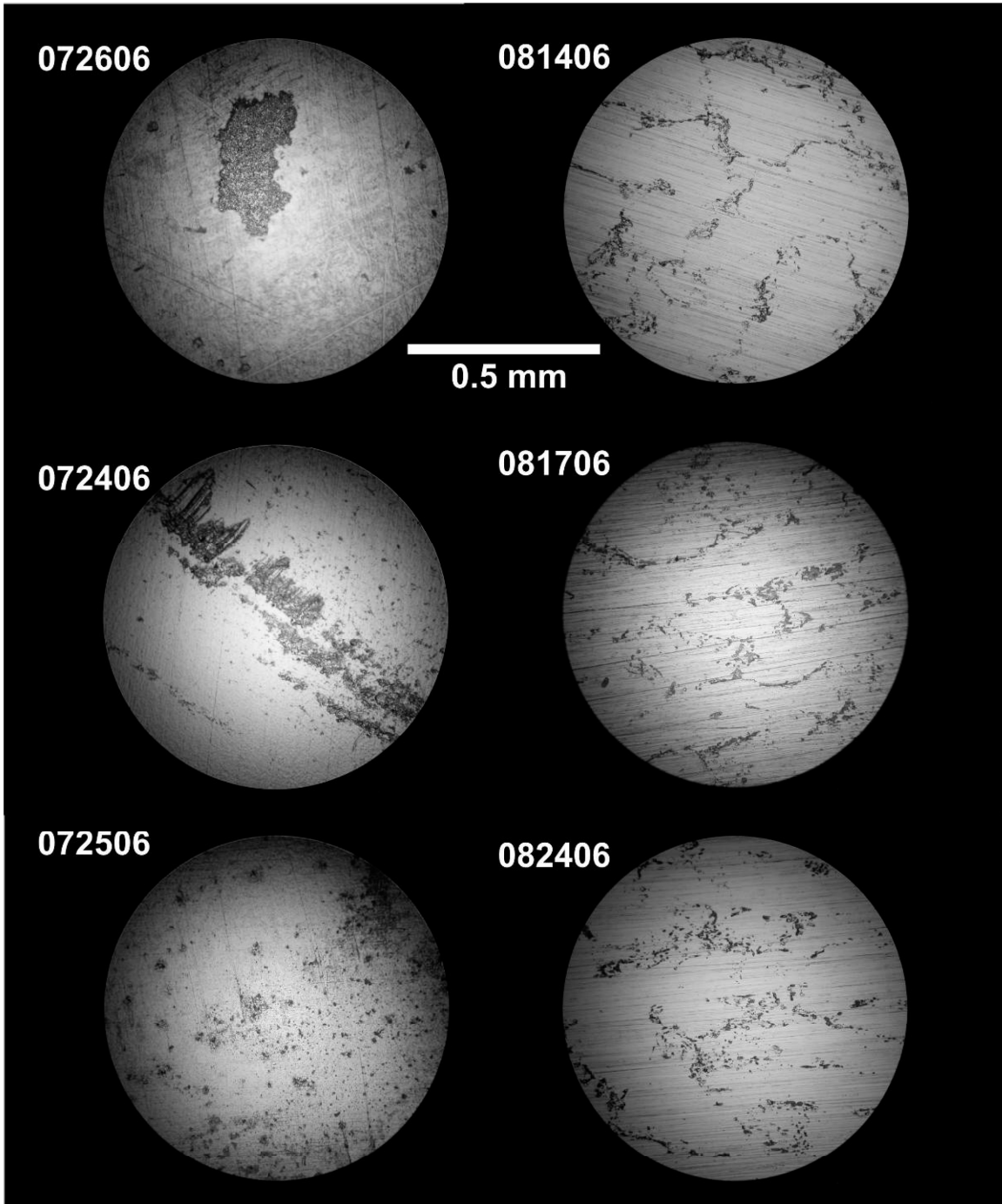


Figure 19. LOM images of selected specimens showing damage to the surface. Tests 072606, 072406, and 072506 are 304B4 specimens, and Tests 081406, 081706, and 082406 are Ni-Cr-Mo-Gd specimens. All images were taken at a magnification factor of 200 $\times$ .

The specimen surfaces were also observed with SEM in both secondary electron (SE) and backscatter electron (BSE) modes. Images of 304B4 are shown in Figure 20. Figure 20A shows a large shallow area of damage while the other images are of smaller pits, less than 100  $\mu\text{m}$  in size. The BSE images show the numerous  $\text{Cr}_2\text{B}$  phases (darker grey) in the material. The darker areas are corrosion sites or accumulated